FINAL REPORT: NASA Contract No. NASW–4806

Determination of Hydrocarbon Abundances and the Strength of Eddy Mixing in the Stratosphere of Neptune: Analysis of UVS Solar Occultation Lightcurves

13 November 1995

James Bishop
Computational Physics Incorporated, Fairfax, Virginia

SUMMARY

Work completed during contract:

1. Completed writing and editing of "The Middle and Upper Atmosphere of Neptune", by J. Bishop, S. K. Atreya, P. N. Romani, G. S. Orton, B. R. Sandel, and R. V. Yelle, to appear as a chapter in the book *Neptune and Triton*, D. Cruikshank and M. S. Matthews, eds., University of Arizona Press. (In press, see Attachment 1).

2. Completed work on UVS occultation lightcurve modeling using photochemical models fitting ground-based and Voyager IRIS infrared data. This work is documented in the attached DPS poster materials (Bishop et al. 1994) (Attachment 2).

3. Supported the Voyager IRIS data modeling by Romani et al. (1993) (see Attachment 3).

TASKS ACCOMPLISHED

While it was a distinct honor to have been asked to take the lead in compiling a review chapter, it was a very time-consuming task. I believe that we managed to structure the presentation so as to be suitable for persons entering this field of study (*e.g.*, students and post-docs) while covering all the pertinent topics in sufficient detail to be useful as a technical review. The galleys were checked and corrected for the final time back in February 1995 (see Attachment 1).

Work on completing our analysis of the Voyager UVS solar occultation data acquired during Neptune encounter is essentially complete, as testified by the attached poster materials (Attachment 2). These materials provide a self-contained summary of our achievements in this area. A paper has been in preparation for some time, and requires only about a week's worth of effort to complete; this will be returned to in December of this year, and submission of the paper to *Journal of Geophysical Research – Planets* should occur in January. The photochemical modeling addresses the recent revision in branching ratios for radical production in the photolysis of methane at H Lyman α implied by the lab measurements of Mordaunt et al. (1993). It should be noted that Mordaunt et al. did not present definitive branching ratios but instead simply demonstrated that methyl production occurs about half the time; the branching ratios for production of other radicals are still uncertain, so that it is necessary to ascertain the variation in modeling results associated with the Mordaunt et al. uncertainties. As it turns out, the modification of CH_4 branching ratios suggested by the Mordaunt et al. results (discussed in the poster materials) does not lead to significantly different photochemical modeling results compared with modeling incorporating the branching ratios advocated by Slanger and Black (1982). Yelle et al. (1993) carried out an independent analysis of the UVS occultation lightcurves using "objective" inversion techniques similar in spirit to the techniques we applied in our analysis of the Uranian solar occultation data (Bishop et al. 1990). We had initially tried to apply these techniques to the Neptune data but found the data to be too noisy for reliable results, contrary to the claims of Yelle et al. Instead, we rely on the forward modeling approach described in Bishop et al. (1992), augmented with a more thorough incorporation of the Romani et al. (1993) photochemical model. While claiming to address photochemical issues, Yelle et al. did not carry out photochemical modeling calculations but rather relied on back-of-the-envelope estimates for column production and loss rates and product species fluxes (principally ethane, C_2H_6) that are highly questionable. The results of their analysis were forcefully presented; nevertheless, it has been necessary to assess their conclusions carefully to avoid placing too much reliance upon them.

The software generated in this effort has been useful for checking the degree to which photochemical models addressing other datasets (mainly infrared) are consistent with the UVS data. This is documented in the Romani et al. (1993) paper (Attachment 3). This work complements the UVS modeling results in that the IR data refer to deeper pressure levels ($p > 0.1$ mbar); as regards the modeling of UVS data, the most significant result is the convincing support for the presence of a stagnant lower stratosphere. Evidence for strong dynamical (mixing) transport of minor constituents at shallower pressures is provided by the

UVS data analysis, as discussed in the Attachment 2 materials.

All aspects of this work were carried out in close collaboration with Dr. Paul N. Romani (NASA/GSFC).

References

Bishop, J., S. K. Atreya, F. Herbert, and P. Romani 1990. Reanalysis of Voyager 2 UVS occultations at Uranus: Hydrocarbon mixing ratios in the equatorial stratosphere. *Icarus* **88**:448–464.

Bishop, J., S. K. Atreya, P. N. Romani, B. R. Sandel, and F. Herbert 1992. Voyager 2 ultraviolet spectrometer solar occultations at Neptune: Constraints on the abundance of methane in the stratosphere. *J. Geophys. Res.* **97**:11681–11694.

Bishop, J., P. N. Romani, and S. K. Atreya 1994. Photochemical modeling of Voyager UVS solar occultation lightcurves acquired at Neptune. *BAAS* **26**:1095.

Mordaunt, D. H., I. R. Lambert, G. P. Morley, M. N. R. Ashfold, R. N. Dixon, C. M. Western, L. Schnieder, and K. H. Welge 1993. Primary product channels in the photodissociation of methane at 121.6 nm. *J. Chem. Phys.* **98**:2054–2065.

Romani, P. N., J. Bishop, B. Bézard, and S. Atreya 1993. Methane photochemistry on Neptune: Ethane and acetylene mixing ratios and haze production. *Icarus* **106**:442–463.

Slanger, T. G., and G. Black 1982. Photodissociative channels at 1216 Å for H_2O, NH_3, and CH_4. *J. Chem. Phys.* **77**:2432–2437.

Yelle, R. V., F. Herbert, B. R. Sandel, R. J. Vervack, Jr., and T. M Wentzel 1993. The distribution of hydrocarbons in Neptune's upper atmosphere. *Icarus* **104**:38–59.

TEX Format Date: January 18, 1995; Time: 8:32

Author Page Proof
MASTER PROOF

THE MIDDLE AND UPPER ATMOSPHERE OF NEPTUNE

JAMES BISHOP
Computational Physics Incorporated

SUSHIL K. ATREYA
University of Michigan

PAUL N. ROMANI
NASA Goddard Space Flight Center

GLENN S. ORTON
Jet Propulsion Laboratory

and

BILL R. SANDEL and ROGER V. YELLE
University of Arizona

Observations pertaining to the middle and upper atmosphere of Neptune obtained from Earth have, until recently, been limited to hydrocarbon thermal emission spectra and refractive stellar occultations. The Voyager 2 encounter provided our first detailed look at these atmospheric regions. RSS and IRIS measurements have confirmed the $p-T$ structure near the tropopause inferred from pre-Voyager infrared measurements but have also revealed a steeper temperature gradient at smaller pressures and pronounced latitudinal variations, with tropopause temperatures in the range 50 K to 57 K. The pre-Voyager estimate of a stratospheric methane mixing ratio of 2%, more than 2 orders of magnitude in excess of the tropopause cold trap value, has been revised downward considerably (10^{-4}–10^{-3}) but oversaturation is still indicated. In contrast, Voyager measurements of stratospheric C_2H_2 and C_2H_6 abundances are in very close agreement with estimates from Earth-based observations: $\sim 6 \times 10^{-8}$ and $\sim 1.5 \times 10^{-6}$, respectively, near 0.5 mbar ($T \approx 160$ K). Vertical transport in the upper stratosphere is fairly vigorous, with eddy mixing coefficient values in the range 3 to 10×10^6 cm^2 s^{-1} near the 0.2 μbar level as determined from the UVS solar occultation data. Eddy mixing in the lower stratosphere ($p \gtrsim 2$ mbar) is sluggish by comparison, with values on the order of 1 to 3×10^3cm^{2}s^{-1} indicated by photochemical modeling of the infrared emission spectra. Submillimeter emissions by HCN and CO in the stratosphere, first detected in 1991, have raised new questions regarding stratospheric chemistry and transport on Neptune; modeling of the abundances of these species, in conjunction with continued photochemical modeling of hydrocarbon thermal emissions and the UVS solar occultation data, is likely to lead to a characterization of eddy mixing throughout the stratosphere and to tighter constraints on stratospheric N_2 and CH_4 mixing ratios. Other prominent modeling issues of current interest are

ATTACHMENT 1

PHOTOCHEMICAL MODELING OF VOYAGER UVS SOLAR OCCULTATION LIGHTCURVES ACQUIRED AT NEPTUNE

James Bishop (Computational Physics Inc.)
Paul N. Romani (NASA/Goddard Space Flight Center)
Sushil K. Atreya (University of Michigan)

Ingress and egress occultations of the Sun by Neptune were recorded with the UVS instrument on Voyager 2 [Broadfoot *et al.* 1989]. Previous modeling of the 125–140 nm lightcurves indicated eddy mixing coefficient values of $3-10\times10^{6}$ cm^2 s^{-1} near the 0.2 μbar level and methane mixing ratios in the lower stratosphere on the order of $1-3\times10^{-4}$ [Bishop *et al.* 1992]. These results should be insensitive to photochemical details, provided methane is the main source of opacity at these wavelengths. The UVS lightcurves at longer wavelengths (140–153 nm) are expected to be dominated by the opacity of C_2 species (ethane, acetylene, ethylene) and perhaps higher order organics. At still longer wavelengths, H_2 Rayleigh scattering is a major opacity source. We will present photochemical models giving good agreement with both sets of UVS lightcurves at wavelengths 125–165 nm and with C_2H_6 and C_2H_2 abundances near 0.5 mbar derived from IRIS measurements [Bézard *et al.* 1991]. The current photochemical model incorporates several updates, including the recent revision in CH_4 photolysis branching ratios at Lyman α [Mordaunt *et al.* 1993]. These model fits strongly suggest a region of enhanced eddy mixing near the 10 μbar level ($K \gtrsim 10^8$ cm^2 s^{-1}), decreasing at higher altitudes. Comparisons between egress ($\sim$ 49°S latitude) and ingress (61°N) UVS results will be discussed, as well as the impact of uncertainties in mean stratospheric temperature and key reaction rates. In line with our earlier work, methane mixing ratios on the order of 10^{-4} are required to obtain good agreement between the photochemical models and the UVS lightcurves.

This work supported by NASA Contract NASW-4806.

UVS LIGHTCURVES

The UVS solar occultation lightcurves relevant to stratospheric investigations fall into three groups: for $\lambda_c \lesssim 138$ nm, the lightcurves exhibit half-light points in the 0.1–0.3 μbar region, those with $138 \lesssim \lambda_c \lesssim 153$ nm probe progressively deeper into the stratosphere, while the half-light points of $\lambda_c \gtrsim 153$ nm lightcurves are at pressures $\gtrsim 0.1$ mbar. In the figure below, a subset of the UVS solar occultation data used in our modeling is shown as transmission lightcurves ($I(z_\perp, \lambda_c)/I_o(\lambda_c)$, where $z_\perp$ is the minimum tangent ray height) averaged over 0.96 s intervals and ordered according to the channel center wavelengths λ_c at 500 km MTRH. Altitude resolutions are 9.5 km (ingress) and 12.3 km (egress), and the spectral resolution is ~2.5 nm. The apparent solar diameter for both occultations (~4 km at ingress, ~20 km at egress) is small relative to the MTRH range over which total opacities drop from 0.9 to 0.1 and can be ignored. Other aspects of the occultation (*e.g.*, channel center offsets as functions of MTRH stemming from the limit cycle motion, convolution of model transmission spectra at 0.1 nm resolution with the UVS slit function) are incorporated in our modeling using the information provided to us by B. Sandel and R. Vervack (Univ. of Arizona).

In addition to measurement noise, the data are afflicted by two main sources of error: internal instrument scattering, primarily of the solar Lyman α line, and pointing errors which introduce uncertainties in the ratioing. These errors and the derivation of a corresponding standard deviation σ_D are discussed by Yelle *et al.* [1993]. In recognition of this, we display the UVS data as data ranges defined by $I(z_\perp, \lambda_c)/I_o(\lambda_c) \pm \sigma_D$ when making comparisons with model lightcurves.

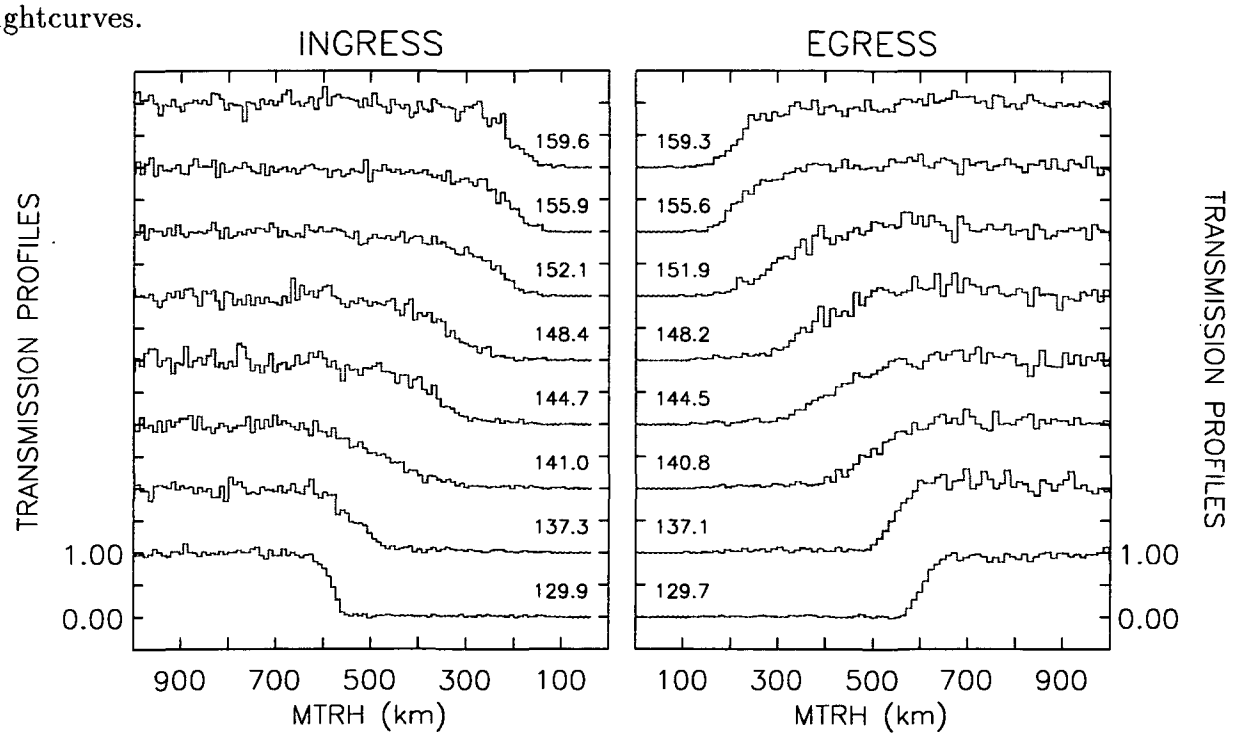

IRIS Results: The IRIS measurements of stratospheric hydrocarbon emissions analyzed by Bézard *et al.* [1991] yielded acetylene and ethane mixing ratios of $\sim 4 \times 10^{-8}$ (0.2 mbar) and $\sim 1.3 \times 10^{-6}$ (0.7 mbar), respectively; these results are based on a large selection of low spatial resolution data with field-of-view centers ranging from 10°S to 50°S latitude. Since the UVS egress occultation latitude lies within this range, the IRIS-derived mixing ratios have been used to help identify successful photochemical models under egress conditions.

MODELING PROCEDURE

The model lightcurves are constructed using the H_2 density distributions provided by the model atmospheres and hydrocarbon (CH_4, C_2H_2, C_2H_4, C_2H_6) density distributions obtained from solving the 1-D continuity equation

$$\frac{d\Phi_i}{dz} = P_i - L_i$$

for each species i assuming steady-state conditions. (Variables are defined below). In terms of the mixing ratio for species i, the flux is

$$\Phi_i = -N(D_i + K)\frac{df_i}{dz} - D_i N f_i (H_i^{-1} - H_{atm}^{-1}).$$

Once the hydrocarbon abundances are evaluated, simulated UVS lightcurves are given by

$$\overline{I}(r_\perp, \lambda_c) = \int_{\lambda_c - \Delta_s\lambda}^{\lambda_c + \Delta_s\lambda} R(\lambda - \lambda_c) \cdot I_o(\lambda) \cdot \exp\left[-2\int_{r_\perp}^{\infty} dr \cdot \frac{r}{(r^2 - r_\perp^2)^{1/2}} \cdot n(z) \cdot \sum_i f_i(z)\sigma_i(\lambda)\right]$$

The main fitting parameters are the mixing ratio of methane in lower stratosphere ($f_T(CH_4)$) and the parameters defining the eddy mixing coefficient profile. We have explored several different types of K profiles. In seeking out successful model fits, our first step is to identify ($f_T(CH_4)$, $K_{1/2}(\lambda_c < 140$ nm)) pairs providing the best agreement with the UVS data at wavelengths shortwards of 140 nm; $K_{1/2}(\lambda_c)$ is the eddy mixing coefficient at the half-light point of channel λ_c. As previously mentioned, these lightcurves are expected to be least sensitive to photochemical modeling details. Using the constraints on $f_T(CH_4)$ and the strength of eddy mixing at the top of the region probed by the UVS lightcurves, the K profile is then varied (as allowed by the adopted form) to try to obtain agreement at longer wavelengths, which probe progressively deeper pressures.

Variable Definitions

f_i	mixing ratio of species i
Φ_i	vertical flux of species i (molecules cm^{-2} s^{-1})
P_i	chemical production rate of species i (molecules cm^{-3} s^{-1})
L_i	chemical loss rate of species i (molecules cm^{-3} s^{-1})
D_i	molecular diffusion coefficient of species i for H_2–He atmosphere (cm^2 s^{-1})
K	atmospheric eddy mixing coefficient (cm^2 s^{-1})
H_i	partial pressure scale height of species i
H_{atm}	pressure scale height of the background atmosphere
z, r	altitude, radial distance from center of planet
$z_\perp$, $r_\perp$	minimum tangent ray height for line of sight to center of solar disk
λ	wavelength
λ_c	channel center wavelength at $z_\perp$
$\Delta_s\lambda$	UVS channel spectral width
$R(\lambda - \lambda_c)$	normalized instrument response at λ in channel with center wavelength λ_c
I_o	solar flux at top of atmosphere (photons cm^{-2} s^{-1} Å^{-1})
σ_i	photoabsorption cross section of species i (cm^2)
n	atmospheric number density at altitude z (cm^{-3})

ATMOSPHERE MODELS

In our modeling, we adopt a mean molecular weight of 2.393 [Conrath *et al.* 1991] with a helium mixing ratio $f(\mathrm{He})$ of 0.19. Atmospheric pressure-temperature ($p-T$) profiles at pressures deeper than ~ 2 mbar at the ingress and mean egress latitudes are taken from Lindal [1992]. These are extended to 1.0 μbar using a profile of the form presented by Hubbard *et al.* [1987]; after scaling to $f(\mathrm{He}) = 0.19$, their analysis of the 20 August 1985 stellar occultation central flash indicates a temperature of 143 K near 0.42 mbar. The nominal 1 μbar temperature is 168 K, taken from Orton *et al.* [1992]. The high altitude segment is based on the preliminary analysis of the UVS ingress solar occultation data presented by Broadfoot *et al.* [1989].

Since the $p-T$ profile is not well-constrained by Voyager flyby data at pressures in the range 2 mbar to 0.01 μbar, "warm" and "cool" models have been used in the modeling. These are defined by shifting the 1 μbar temperature of Orton *et al.* by ± 20 K as suggested by numerous stellar occultations [Roques *et al.* 1994]. In these models, the RSS profiles and Hubbard *et al.* 0.42 mbar point are not modified.

The 1 bar radii at the UVS occultation latitudes, which are needed to place the $p-T$ profiles on an altitude scale, are taken from Lindal [1992]: 24443 km at the ingress latitude of 61°N and 24535 km at the mean egress latitude of 49°S. The altitude scale on the right hand ordinate axis in the figure below corresponds to the nominal ingress $p-T$ model.

The region where photochemically produced hydrocarbons are predicted to condense is also indicated [Moses *et al.* 1992; Romani *et al.* 1993].

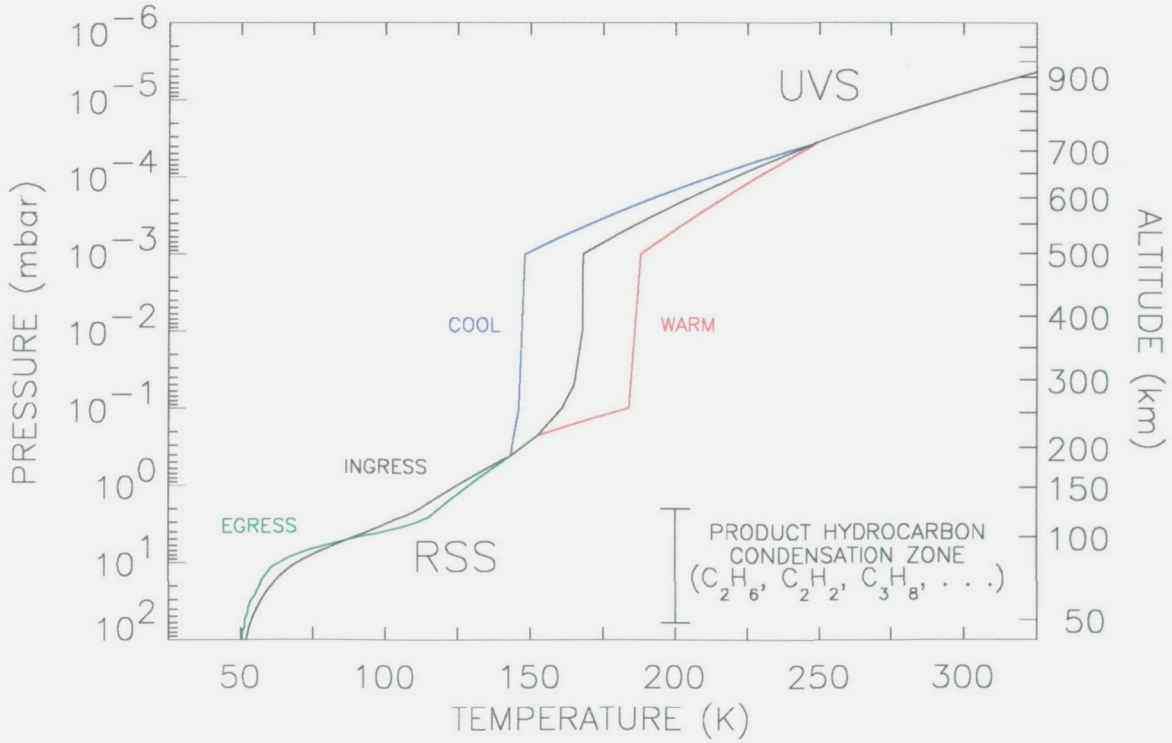

OTHER INPUTS

Solar Irradiance Spectrum

Photolysis rates are calculated using solar irradiance fluxes summed over 10 Å intervals spanning the wavelength range 1000–2500 Å. At wavelengths longward of 1204 Å, the fluxes are from the 1985 Spacelab-2 flight of SUSIM [see Bruckner *et al.* 1993], and a scaled ($F_{10.7} = 207$) Hinterreger spectrum [Hinteregger *et al.* 1981] is used at shorter wavelengths. The composite spectrum at 1 AU is shown below and is representative of solar maximum conditions; the line-integrated Lyman α flux is 6.5×10^{11} ph cm^{-2} s^{-1}. At Neptune's distance from the Sun, the pervasive Lyman α skyglow associated with the local interstellar medium is not negligible and has been included in the modeling; based on near-encounter LISM measurements by the Voyager UVS, the contribution to the CH_4 photolysis rate is 3×10^{-9} s^{-1} (at the top of the atmosphere). The SUSIM spectrum at 1 Å resolution is also employed in the lightcurve modeling.

In our modeling, we adopt "local" conditions, *i.e.*, we adopt model atmospheres and evaluate photolysis rates corresponding to conditions at the occultation latitudes at the time of encounter. Our modeling of the UVS lightcurves suggest rapid eddy mixing at pressures 1 μbar $\lesssim p \lesssim$ 0.1 mbar, so that the timescale for mixing ($\tau_{\rm mix} = H_n^2/K$, where H_n is the local atmospheric density scale height and K is the eddy mixing coefficient) is significantly smaller that a solar cycle (and consequently much shorter than a Neptune season). The alternate analysis of the UVS data by Yelle *et al.* [1993] suggests $K \approx 10^5$ cm^2 s^{-1}, which is smaller than the values of K we infer at the same pressures; even with this value, though, the mixing timescales are significantly smaller than seasonal or solar cycle durations. The effective solar zenith angles adopted in the ingress and egress modeling are 89.2° and 40.2°, respectively, corresponding to diurnally averaged solar illumination conditions at the time of encounter.

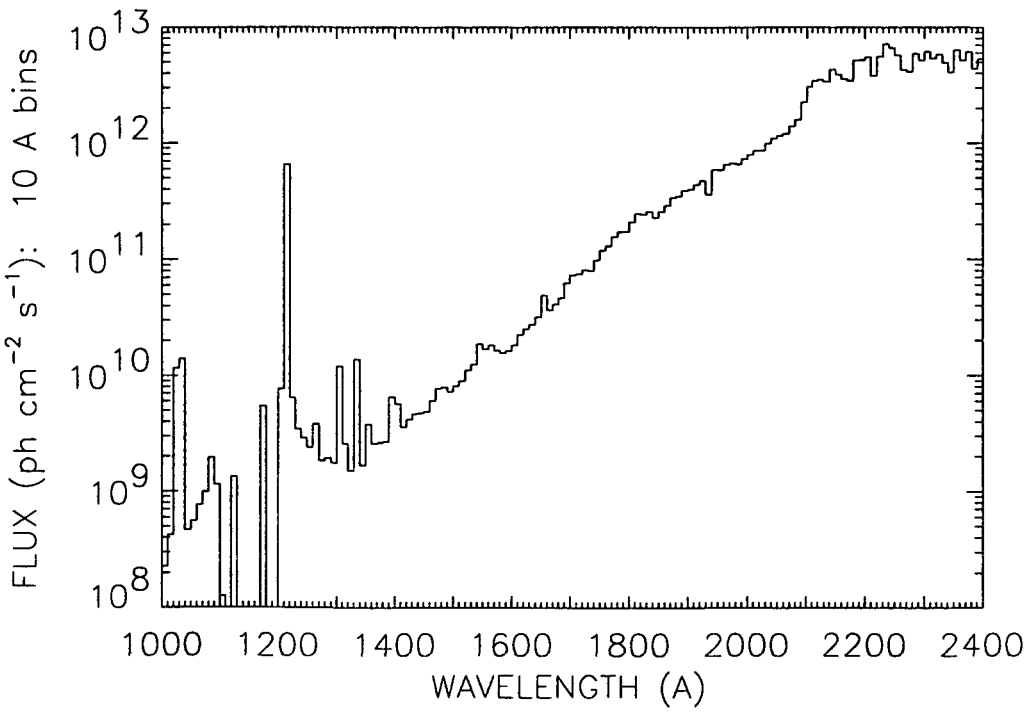

Photoabsorption Cross Sections

The photoabsorption cross sections used in the opacity modeling are shown in the accompanying figure, at roughly 2 Å resolution. These are taken from:

CH_4	Lee and Chiang [1983] & Mount *et al.* [1977]
C_2H_2	Suto and Lee [1984] & Wu *et al.* [1989; personal communication] (at $T = 155$ K)
C_2H_4	R. Wu, personal communication ($T = 155$ K)
C_2H_6	Mount and Moos [1978]
C_4H_2	Glicker and Okabe [*J. Phys. Chem.* **91**:437, 1987]

Superimposed are the cross sections convolved with the UVS instrument slit function. The channel center wavelengths for the ingress occultation data at a tangent altitude of 500 km are also indicated.

The photolysis channels and branching ratios included in the photochemical modeling are listed on the accompanying table. The recent revision in the direct quantum yield of CH_3 from the photolysis of methane at Lyman α has been folded into our modeling. However, since the story of CH_4 Ly-α photolysis is still incomplete, we have attempted to make reasonable estimates of the branching ratios for each energy-allowed channel. These estimates are discussed in detail on the accompanying page.

Chemical Reaction Rates

The chemical reactions included in the modeling are listed on the accompanying table along with the adopted rates. There have been several updates to the modeled chemical scheme since the study by Romani *et al.* [1993]. The most notable changes are (1) the introduction of the photolysis channel $CH_4 + h\nu \rightarrow CH_3 + H$ using the results of Mordaunt *et al.* [1993] and (2) revision of the chemical pathways involving the vinyl radical (C_2H_3) (see talk by Romani *et al.*, this meeting). The chemical scheme is relatively complete for the C_2 hydrocarbons (see figure). Expanding the chemical scheme to a more complete coverage of reaction paths involving C_3 and C_4 species, similar to the photochemical model presented by Moses *et al.* [1992], will be carried out in the near future.

Condensation

In the lower stratosphere, temperatures are cold enough to result in very large supersaturations (S) for several hydrocarbon species (principally C_2H_6 and C_2H_2) if these remained in the gas phase. Consequently, a condensation loss is included. Our handling of this loss mechanism is discussed in detail in Romani *et al.* [1993]; the nominal placement for removal from the gas phase is dictated by the condition $S \geq 1$. The study of the relative efficiency of condensation processes by Moses *et al.* [1992] suggests that the condensation levels of product hydrocarbons should lie deeper in the atmosphere than indicated by the $S \geq 1$ condition; however, both the IRIS and UVS hydrocarbon data refer to pressure levels ($p \approx 0.5$ mbar and $p \lesssim 0.1$ mbar, respectively) well above the condensation levels so that modeling of these data are only indirectly affected by the exact placement of these levels. The important point is the existence of an efficient loss mechanism acting at a deeper level that establishes downward fluxes of acetylene and ethane in the pressure regions sounded by the IRIS and UVS data.

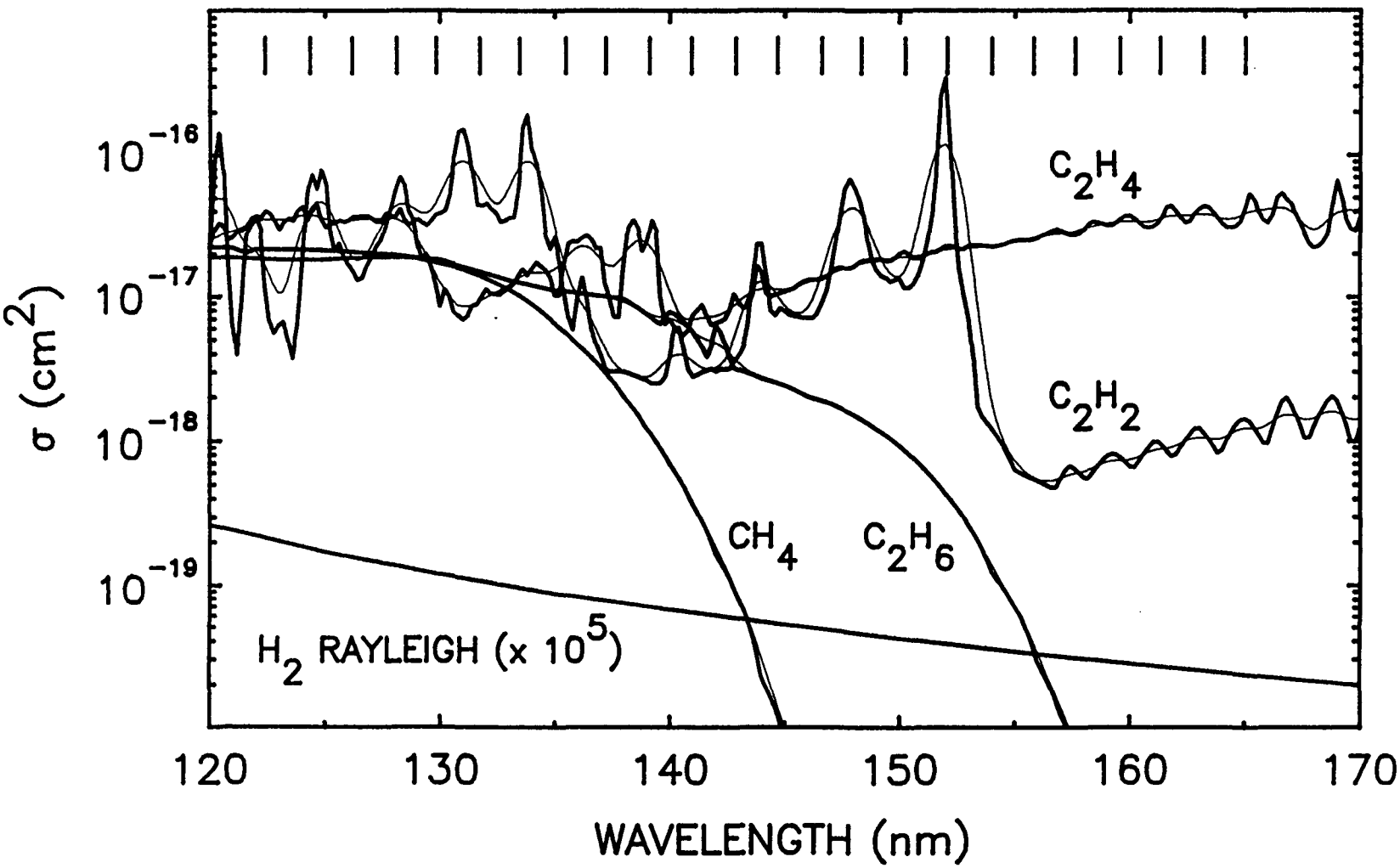
10^{-16}
10^{-17}
10^{-18}
10^{-19}
σ (cm^2)
C_2H_4
C_2H_2
CH_4
C_2H_6
H_2 RAYLEIGH (x 10^5)
120
130
140
150
160
170
WAVELENGTH (nm)

PHOTOLYSIS CHANNELS AND REFERENCES

	REACTION	*BRANCHING RATIOS*	*REFERENCES*
J1a	$CH_4 + h\nu \rightarrow {}^3CH_2 + H + H$	$q(121.6) = 0.212$ *** *see text* ***	Lee & Chiang (1983) J. Chem. Phys. 78:688 Mount et al. (1977) Astrophys. J. 214:L47
J1b	$CH_4 + h\nu \rightarrow {}^1CH_2 + H_2$	$q(121.6) = 0.282$	McNesby & Okabe (1964) Adv. in Photochem. 3:157 Calvert and Pitts (1966) Photochemistry, J Wiley & Sons, Inc.
J1c	$CH_4 + h\nu \rightarrow CH + H + H_2$	$q(121.6) = 0.100$	Rebbert & Ausloos (1972) J. Photochem. 1:171 Gorden & Ausloos (1967) J. Chem. Phys. 46:4823
J1d	$CH_4 + h\nu \rightarrow CH_3 + H$	$q(121.6) = 0.406$	Slanger & Black (1982) J. Chem. Phys. 77:2432 Mordaunt et al. (1993) J. Chem. Phys. 98:2054
J1e	$CH_4 + h\nu \rightarrow {}^1CH_2 + H + H$	$q(121.6) = 0.0$	Laufer & McNesby (1968) J. Chem. Phys. 49:2272
J2a	$C_2H_2 + h\nu \rightarrow C_2H + H$	$q(\lambda < 153) = 0.30$ $q(153 < \lambda < 186) = 0.12$ $q(186 < \lambda < 201) = 0.21$	Okabe (1981) J. Chem. Phys. 75:2772 Okabe (1981) J. Chem. Phys. 78:1312 Shin & Michael (1991) J. Phys. Chem. 95:5864 McDonald et al. (1978) Chem. Phys. 33:161
J2b	$C_2H_2 + h\nu \rightarrow C_2 + H_2$	$q(\lambda < 201) = 0.10$	Suto & Lee (1984) J. Chem. Phys. 80:4824 Wu et al. (1989) J. Chem. Phys. 91:272 Nakayama & Watanabe (1964) J. Chem. Phys. 40:558 R. Wu (1991) personal communication
J3a	$C_2H_4 + h\nu \rightarrow C_2H_2 + H_2$	$q(\lambda < 190) = 0.51$	Xia et al. (1991) J. Quant. Spect. Rad. Transfer 45:77 R. Wu (1991) personal communication
J3b	$C_2H_4 + h\nu \rightarrow C_2H_2 + H + H$	$q(\lambda < 190) = 0.49$	Hara & Tanaka (1973) Bull. Chem. Soc. Japan 46:3012 Sauer & Dorfman (1961) J. Chem. Phys. 35:497 Back & Griffiths (1967) J. Chem. Phys. 46:4839

J4a	$C_2H_6 + h\nu \rightarrow C_2H_2 + H_2 + H_2$	$q(121.6) = 0.25$ $q(\lambda < 170) = 0.27$	Mount & Moos (1978) Astrophys. J. 224:L35 Calvert & Pitts (1966) Photochemistry, J. Wiley & Sons, Inc. Akimoto et al. (1965) J. Chem. Phys. 42:3864
J4b	$C_2H_6 + h\nu \rightarrow C_2H_4 + H + H$	$q(121.6) = 0.30$ $q(\lambda < 170) = 0.14$	Lias et al. (1970) J. Chem. Phys. 52:1841 Hampson & McNesby (1965) J. Chem. Phys. 42:2200
J4c	$C_2H_6 + h\nu \rightarrow CH_4 + {}^1CH_2$	$q(121.6) = 0.25$ $q(\lambda < 170) = 0.02$	
J4d	$C_2H_6 + h\nu \rightarrow C_2H_4 + H_2$	$q(121.6) = 0.13$ $q(\lambda < 170) = 0.56$	
J4e	$C_2H_6 + h\nu \rightarrow CH_3 + CH_3$	$q(121.6) = 0.08$ $q(\lambda < 170) = 0.01$	
J5a	$C_4H_2 + h\nu \rightarrow C_4H + H$	$q(\lambda < 166) = 0.20$	Okabe (1981) J. Chem. Phys. 75:2772 Glicker & Okabe (1987) J. Phys. Chem. 91:437
J5b	$C_4H_2 + h\nu \rightarrow C_2H_2 + C_2$	$q(\lambda < 166) = 0.10$ $q(166 < \lambda < 207) = 0.06$	Allan (1984) J. Chem. Phys. 80:6020
J5c	$C_4H_2 + h\nu \rightarrow C_2H + C_2H$	$q(\lambda < 166) = 0.03$ $q(166 < \lambda < 207) = 0.01$	
J5d	$C_4H_2 + h\nu \rightarrow C_4H_2^{**}$	$q(\lambda < 166) = 0.67$ $q(166 < \lambda < 207) = 0.93$ $q(\lambda > 207) = 1.00$	

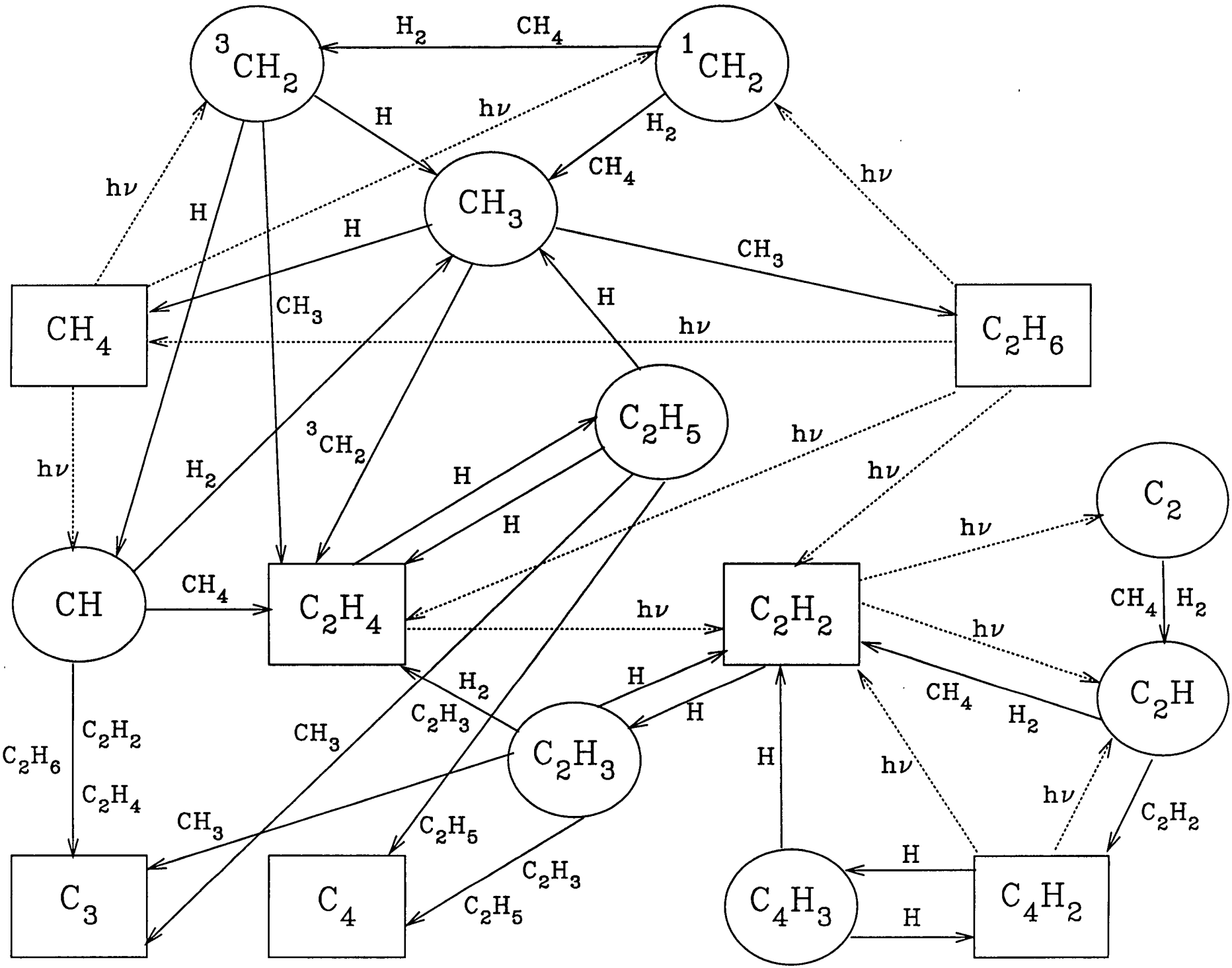
$^3CH_2$
$^1CH_2$
CH_3
CH_4
C_2H_6
C_2H_5
CH
C_2H_4
C_2H_2
C_2H_3
C_2H
C_2
C_3
C_4
C_4H_3
C_4H_2
H
H_2
$h\nu$

REACTIONS, RATES AND REFERENCES

	REACTION	*RATE EXPRESSION*	*REFERENCES*
R1	$^1CH_2 + H_2 \rightarrow CH_3 + H$	$k = 9.24 \times 10^{-11}$	Allen et al. (1992) Icarus 100:527 Langford et al. (1983) J. Chem. Phys. 78:6650 Ashfold et al. (1981) Chem. Phys. 55:245 Baun et al. (1970) J. Chem. Phys. 52:5131
R2	$^1CH_2 + CH_4 \rightarrow CH_3 + CH_3$	$k = 6.0 \times 10^{-11}$	Bohland et al. (1985) Ber. Bunsenges. Phys. Chem. 89:1110
R3	$CH + CH_4 \rightarrow C_2H_4 + H$	$k = 5.0 \times 10^{-11}\, e^{200/T}$ $k_{max} = 1.7 \times 10^{-10}$	Baulch et al. (1992) J. Phys. Chem. Ref. Data 21:411 upper limit is T = 167 K rate from Berman & Lin (1983) Chem. Phys. 82:435
R4	$CH + H_2 \xrightarrow{M} CH_3$	$k_o = 8.75 \times 10^{-31}\, e^{524/T}$ $k_\infty = 8.3 \times 10^{-11}$ $k = \frac{k_\infty k_o M}{k_\infty + k_o M}$	fit to data in Berman & Lin (1984) J. Phys. Chem. 81:5743
R5	$CH_3 + H \xrightarrow{M} CH_4$	$k_o = 4.0 \times 10^{-29}$ $k_\infty = 4.7 \times 10^{-10}$ $k = \frac{k_\infty k_o M}{k_\infty + k_o M} \cdot F$ with $f_C = 0.902 - 1.03 \times 10^{-3}\, T$ and $f_n = 1$	Brouard et al. (1989) J. Phys. Chem. 93:4047
R6	$CH_3 + CH_3 \xrightarrow{M} C_2H_6$	$k_o = 3.5 \times 10^{-7}\, T^{-7.03}\, e^{-1390/T}$ $k_\infty = 6.0 \times 10^{-11}$ $k = \frac{k_\infty k_o M}{k_\infty + k_o M} \cdot F$ with $f_C = 0.38\, e^{-T/73} + 0.62\, e^{-T/1180}$ and $f_n = 0.75 - 1.27 \log_{10} f_C$	Baulch et al. (1992) J. Phys. Chem. Ref. Data 21:411 N.B. bath gas is Ar

R7	$H + H \xrightarrow{M} H_2$	$k = 2.7 \times 10^{-31}\, T^{-0.6}$	Baulch et al. (1992) J. Phys. Chem. Ref. Data 21:411 N.B. bath gas is H2
R8	$H + C_2H_2 \xrightarrow{M} C_2H_3$	$k_o = 3.3 \times 10^{-30}\, e^{-740/T}$ $k_\infty = 1.4 \times 10^{-11}\, e^{-1300/T}$ $k = \frac{k_\infty k_o M}{k_\infty + k_o M} \cdot F$ with $f_C = 0.44$ and $f_n = 0.75 - 1.27 \log_{10} f_C$	Baulch et al. (1992) J. Phys. Chem. Ref. Data 21:411 N.B. bath gas is He
R9	$H + C_2H_3 \rightarrow C_2H_2 + H_2$	$k = 5.0 \times 10^{-11}$	see R64
R10	$H_2 + C_2H_3 \rightarrow C_2H_4 + H$	$k = 5.01 \times 10^{-20}\, T^{2.63}\, e^{-4298/T}$	Tsang & Hampson (1986) J. Phys. Chem. Ref. Data 15:1087 Fahr et al. (1994) in preparation
R11	$H + C_2H_4 \xrightarrow{M} C_2H_5$	$k_o = 2.15 \times 10^{-29}\, e^{-349/T}$ $k_\infty = 4.95 \times 10^{-11}\, e^{-1051/T}$ $k = \frac{k_\infty k_o M}{k_\infty + k_o M}$	Lightfoot & Pilling (1987) J. Phys. Chem. 93:3373 (fast rate)
R12	$H + C_2H_5 \rightarrow CH_3 + CH_3$	$k = 7.95 \times 10^{-11}\, e^{-127/T}$	Pratt & Wood (1984) J. Chem. Soc. Faraday Trans. 80:3419
R13	$^3CH_2 + H \xrightarrow{M} CH_3$	$k_o = 3.1 \times 10^{-30}\, e^{457/T}$ $k_\infty = 1.5 \times 10^{-10}$ $k = \frac{k_\infty k_o M}{k_\infty + k_o M}$	Gladstone (1983) Ph.D. Thesis, Cal. Inst. of Tech.
R14	$CH_3 + {}^3CH_2 \rightarrow C_2H_4 + H$	$k = 7.0 \times 10^{-11}$	Tsang & Hampson (1986) J. Phys. Chem. Ref. Data 15:1087
R15	$^3CH_2 + C_2H_2 \rightarrow$ Products	$k = 1.99 \times 10^{-11}\, e^{-3332/T}$	Bohland et al. (1986) Symp. Int. Combust. Proc. 21:841

R16	$C_2H + H \xrightarrow{M} C_2H_2$	$k_o = 1.26 \times 10^{-18}\, T^{-3.1}\, e^{-721/T}$ $k_\infty = 3.0 \times 10^{-10}$ $k = \frac{k_\infty k_o M}{k_\infty + k_o M}$	Tsang & Hampson (1986) J. Phys. Chem. Ref. Data 15:1087
R17	$C_2H + H_2 \rightarrow C_2H_2 + H$	$k = 1.8 \times 10^{-11}\, e^{-1090/T}$	Koshi et al. (1992) J. Phys. Chem. 96:9839
R18	$C_2H + CH_4 \rightarrow C_2H_2 + CH_3$	$k = 1.7 \times 10^{-11}\, e^{-542/T}$	Opansky et al. (1993) 5th Intl. Cnf. on Lab. Research for Planetary Atmospheres, Boulder CO (poster Ch-01)
R19	$C_2H + C_2H_6 \rightarrow C_2H_2 + C_2H_5$	$k = 3.6 \times 10^{-11}$	Lander et al. (1990) J. Phys. Chem. 94:7759
R20	$C_2H + C_2H_2 \rightarrow C_4H_2 + H$	$k = 1.1 \times 10^{-10}\, e^{28/T}$	Pedersen et al. (1993) J. Phys. Chem. 97:6822
R21	$p\text{-}C_3H_4 + H \rightarrow CH_3 + C_2H_2$	$k = 9.62 \times 10^{-12}\, e^{-1560/T}$	Wagner & Zellnar (1972) Ber. Bunsenges. Phys. Chem. 76:518
R22	$^1CH_2 + H_2 \rightarrow {}^3CH_2 + H_2$	$k = 1.26 \times 10^{-11}$	see R1
R23A	$C_2H_3 + C_2H_3 \rightarrow C_2H_2 + C_2H_4$	$k = 2.4 \times 10^{-11}$	Fahr et al. (1991) J. Phys. Chem. 95:3218
R23B	$C_2H_3 + C_2H_3 \xrightarrow{M} C_4H_6$	$k_o = 1.3 \times 10^{-22}$ $k_\infty = 1.2 \times 10^{-10}$ $k = \frac{k_\infty k_o M}{k_\infty + k_o M}$	k_o: Laufer et al. (1983) Icarus 56:560 k_∞: Fahr et al. (1991) J. Phys. Chem. 95:3218
R24	$C_4H + H_2 \rightarrow C_4H_2 + H$	$k_{24} = k_{17}$	in lieu of firm evidence, estimating that C_4H rates are the same as their C_2H analogues. see: Kiefer et al. (1990) Int. J. Chem. Kin. 22:747 Tanzawa & Gardiner (1980) J. Phys. Chem. 84:236 Frank & Just (1990) Combust. Flame
R25	$C_4H + CH_4 \rightarrow C_4H_2 + CH_3$	$k_{25} = k_{18}$	
R26	$C_4H + C_2H_6 \rightarrow C_4H_2 + C_2H_5$	$k_{26} = k_{19}$	
R27	$C_4H + H \xrightarrow{M} C_4H_2$	$k_{27} = k_{16}$	
R28	$C_4H + C_2H_2 \rightarrow C_6H_2 + H$	$k_{28} = k_{20}$	

R29	$C_4H + C_4H_2 \rightarrow C_8H_2 + H$	$k_{29} = k_{20}$	in lieu of firm evidence, estimating that $C_4H + C_4H_2$
R30	$C_2H + C_4H_2 \rightarrow C_6H_2 + H$	$k_{30} = k_{20}$	and $C_2H + C_4H_2$ have the same rate as R20 (see references for R24–R28)
R31	$C_4H_2^{**} + C_4H_2 \rightarrow C_8H_2 + H_2$	$k = 1.5 \times 10^{-10}$	estimating to be kinetic rate limit
R32	$C_4H_2 + H \xrightarrow{M} C_4H_3$	$k_o = 1.0 \times 10^{-26}$ $k_\infty = 1.39 \times 10^{-10}\, e^{-1184/T}$ $k = \frac{k_\infty k_o M}{k_\infty + k_o M}$	Nava et al. (1986) J. Geophys. Res. 91:4585 N.B. k_o is an estimate and also a lower limit
R33	$C_4H_3 + H \rightarrow C_4H_2 + H_2$	$k = 1.2 \times 10^{-11}$	Yung et al. (1984) Astrophys. J. Supp. 55:465
R34	$C_4H_3 + H \rightarrow C_2H_2 + C_2H_2$	$k = 3.3 \times 10^{-11}$	Yung et al. (1984) Astrophys. J. Supp. 55:465
R35	$C_2 + H_2 \rightarrow C_2H + H$	$k = 1.77 \times 10^{-10}\, e^{-1469/T}$	Pitts et al. (1982) Chem. Phys. 68:417
R36	$C_2 + CH_4 \rightarrow C_2H + CH_3$	$k = 5.05 \times 10^{-11}\, e^{-297/T}$	Pitts et al. (1982) Chem. Phys. 68:417
R37	$C_2H + C_2H_4 \rightarrow C_4H_4 + H$	$k = 1.3 \times 10^{-10}$	Lander et al. (1990) J. Phys. Chem. 94:7759
R38	$C_2H_5 + C_2H_5 \rightarrow C_2H_6 + C_2H_4$	$k = 2.4 \times 10^{-12}$	Baulch et al. (1992) J. Phys. Chem. Ref. Data 21:411
R39	$^3CH_2 + {}^3CH_2 \rightarrow C_2H_2 + H + H$	$k = 3.1 \times 10^{-10}$	Darwin (1989) Ph.D. Thesis, Univ. of Calif. Berkeley
R40	$^1CH_2 + CH_4 \rightarrow {}^3CH_2 + CH_4$	$k = 1.2 \times 10^{-11}$	see R2
R41	$CH_3 + C_2H_3 \rightarrow CH_4 + C_2H_2$	$k = 3.4 \times 10^{-11}$	Fahr et al. (1991) J. Phys. Chem. 95:3218

R42	$CH_3 + C_2H_5 \rightarrow CH_4 + C_2H_4$	$k = 1.28 \times 10^{-11}\, T^{-0.32}$	Tsang & Hampson (1986) J. Phys. Chem. Ref. Data 15:1087 Baulch et al. (1992) J. Phys. Chem. Ref. Data 21:411 estimating that $k_{42} = 0.04 \cdot k_\infty$ from R60
R43	$C_2H_5 + H \xrightarrow{M} C_2H_6$	$k_o = 5.5 \times 10^{-23}\, T^{-2}\, e^{-1040/T}$ $k_\infty = 1.5 \times 10^{-13}\, e^{-440/T}$ $k = \frac{k_\infty k_o M}{k_\infty + k_o M}$	Gladstone (1983) Ph.D. Thesis, Cal. Inst. of Tech.
R44	$CH_4 + C_2H_3 \rightarrow CH_3 + C_2H_4$	$k = 2.4 \times 10^{-24}\, T^{4.02}\, e^{-2754/T}$	Tsang & Hampson (1986) J. Phys. Chem. Ref. Data 15:1087
R45	$^3CH_2 + H \rightarrow CH + H_2$	$k = 4.7 \times 10^{-10}\, e^{-370/T}$	Zabarnick et al. (1986) J. Chem. Phys. 85:4373
R46	$C_2H_3 + C_2H_5 \xrightarrow{M} 1\text{-}C_4H_8$	$k = 1.9 \times 10^{-27}$ $k = 2.5 \times 10^{-11}$ $k = \frac{k_\infty k_o M}{k_\infty + k_o M}$	k_o: Laufer et al. (1983) Icarus 56:560 k_∞: Tsang & Hampson (1986) J. Phys. Chem. Ref. Data 15:1087
R47	$C_2H_3 + C_2H_5 \rightarrow C_2H_4 + C_2H_4$	$k = 2.81 \times 10^{-12}$	estimating that the disproportion to recombination ratio is 0.23 (average of C_2H_3 and C_2H_5 self reactions, 0.3 and 0.15 respectively, from Tsang & Hampson (1986) J. Phys. Chem. Ref. Data 15:1087) and taking $k_{48} = k_{47}$
R48	$C_2H_3 + C_2H_5 \rightarrow C_2H_2 + C_2H_6$	$k_{48} = k_{47}$	
R49	$^3CH_2 + C_2H_5 \rightarrow CH_3 + C_2H_4$	$k = 3.0 \times 10^{-11}$	Tsang & Hampson (1986) J. Phys. Chem. Ref. Data 15:1087
R50	$^3CH_2 + C_2H_3 \rightarrow CH_3 + C_2H_2$	$k = 3.0 \times 10^{-11}$	Tsang & Hampson (1986) J. Phys. Chem. Ref. Data 15:1087

R51	$C_2H_5 + C_2H_5 \xrightarrow{M} C_4H_{10}$	$k_o = 6.59 \times 10^{-6}\, T^{-6.39}\, e^{-301/T}$ $k_\infty = 1.9 \times 10^{-11}$ $k = \frac{k_\infty k_o M}{k_\infty + k_o M}$	k_o: Laufer et al. (1983) Icarus 56:560, as reported in the NIST Chemical Kinetics Database V5.0. N.B. Laufer et al. presented tabular data; the NIST equation reproduces the Laufer et al. values to $\sim 1\%$ k_∞: Baulch et al. (1992) J. Phys. Chem. Ref. Data 21:411
R52	$CH + C_2H_2 \rightarrow C_3H_2 + H$	$k = 3.5 \times 10^{-10}\, e^{61/T}$ $k_{max} = 5.3 \times 10^{-10}$	Baulch et al. (1992) J. Phys. Chem. Ref. Data 21:411 upper limit is T = 171 K rate from Berman et al. (1982) Chem. Phys. 73:27
R53 R54	$CH + C_2H_4 \rightarrow p\text{-}C_3H_4 + H$ $CH + C_2H_4 \rightarrow a\text{-}C_3H_4 + H$	$k = 2.2 \times 10^{-10}\, e^{173/T}$ $k_{max} = 7.1 \times 10^{-10}$ $F = 0.5$ $k_{53} = F \cdot k$ $k_{54} = (1 - F) \cdot k$	Baulch et al. (1992) J. Phys. Chem. Ref. Data 21:411 upper limit is T = 160 K rate from Berman et al. (1982) Chem. Phys. 73:27 N.B. rate is split between the two isomers by factor F.
R55	$CH + C_2H_6 \rightarrow$ Products	$k = 1.8 \times 10^{-10}\, e^{132/T}$ $k_{max} = 4.4 \times 10^{-10}$	Baulch et al. (1992) J. Phys. Chem. Ref. Data 21:411 upper limit is T = 162 K rate from Berman & Lin (1983) Chem. Phys. 82:435
R56	$p\text{-}C_3H_4 + H \xrightarrow{M} C_3H_5$	$k_o = 1.636 \times 10^{-26}\, T^{-1.165}$ $k_\infty = 6.0 \times 10^{-11}\, e^{-1233/T}$ $k = \frac{k_\infty k_o M}{k_\infty + k_o M}$	Whytock et al. (1976) J. Chem. Phys. 65:191 Wagner & Zellnar (1972) Ber. Bunsenges. Phys. Chem. 76:518
R57	$C_2H_3 + C_2H_5 \rightarrow CH_3 + C_3H_5$	$k = 2.5 \times 10^{-11} - k_{46}$	Tsang & Hampson (1986) J. Phys. Chem. Ref. Data 15:1087 estimating that $k_{46} + k_{57} = k_\infty$ from R46

R58	$CH_3 + C_2H_3 \rightarrow C_3H_5 + H$	$k_o = 1.3 \times 10^{-22}$	k_o: Laufer et al. (1983) Icarus 56:560
R59	$CH_3 + C_2H_3 \xrightarrow{M} C_3H_6$	$k_\infty = 1.2 \times 10^{-10}$	k_∞: Fahr et al. (1991) J. Phys. Chem. 95:3218
		$k_{59} = \frac{k_\infty k_o M}{k_\infty + k_o M}$	k_{58}: Tsang & Hampson (1986) J. Phys. Chem. Ref. Data 15:1087
		$k_{58} = 0.002 \cdot k_\infty$	
R60	$CH_3 + C_2H_5 \xrightarrow{M} C_3H_8$	$k_o = 1.01 \times 10^{20}\, T^{-16.1}\, e^{-1897/T}$	k_o: Laufer et al. (1983) Icarus 56:560, as reported in the NIST Chemical Kinetics Database V5.0. N.B. Laufer et al. presented tabular data; the NIST equation reproduces the Laufer et al. values to $\sim 30\%$
		$k_\infty = 3.2 \times 10^{-10}\, T^{-0.32}$	k_∞: Tsang (1989) Combust. Flame 78:71
		$k = \frac{k_\infty k_o M}{k_\infty + k_o M}$	
R61	$CH + H_2 \rightarrow {}^3CH_2 + H$	$k = 2.38 \times 10^{-10}\, e^{-1760/T}$	Zabarnick et al. (1986) J. Chem. Phys. 85:4373
R62	$H + C_2H_5 \rightarrow C_2H_4 + H_2$	$k = 3.0 \times 10^{-12}$	Tsang & Hampson (1986) J. Phys. Chem. Ref. Data 15:1087
R63	$CH + H \rightarrow C + H_2$	$k = 1.4 \times 10^{-11}$	Becker et al. (1989) Chem. Phys. Lett. 154:342
R64	$H + C_2H_3 \xrightarrow{M} C_2H_4$	$k_o = 1.49 \times 10^{-27}$	Fahr et al. (1991) J. Phys. Chem. 95:3218
		$k_\infty = 1.55 \times 10^{-10}$	Heinemann et al. (1988) Symp. Int. Combust. Proc. 21:865
		$k = \frac{k_\infty k_o M}{k_\infty + k_o M}$	Monks et al. (1994) in preparation

Notes:

two body rates are in units of cm^3 $molecule^{-1}$ s^{-1}

three body rates are in units of cm^6 $molecule^{-2}$ s^{-1}

if f_C and f_n values are presented, then the factor F is given by

$$\log_{10} F = \frac{\log_{10} f_C}{1 + \left[\frac{\log_{10}\left(\frac{k_0 M}{k_\infty}\right)}{f_n}\right]^2}$$

where M is the background atmosphere number density

QUANTUM YIELDS IN METHANE PHOTOLYSIS

The recent work of Mordaunt *et al.* [1993] by itself is incomplete, in that it does not provide sufficient information to unequivocally assign branching ratios (q) at Lyman α for all possible photolysis channels:

$$\begin{aligned} CH_4 + h\nu &\xrightarrow{a} {}^3CH_2 + H + H \\ &\xrightarrow{b} {}^1CH_2 + H_2 \\ &\xrightarrow{c} CH + H_2 + H \\ &\xrightarrow{d} CH_3 + H \\ &\xrightarrow{e} {}^1CH_2 + H + H \end{aligned}$$

Furthermore, no measurements of ${}^3CH_2$ or ${}^1CH_2$ quantum yields are available and the data we currently have on CH_3, CH, H_2, and H yields are contradictory. The experimental results on which we rely in our attempt to derive reasonable estimates of the branching ratios at 121.6 nm are:

- net CH_3 yield of 0.5 [Mordaunt *et al.* 1993].
- net H_2 yield of 0.5 [Laufer & McNesby 1968]. *Note*: the experiment was actually performed at 123.6 nm with a reported quantum yield of 0.58, giving rise to the contradiction that $q_b + q_c = 0.58$ but $q_d = 0.50$.
- net H yield of 1.0 [Slanger & Black 1982].
- net CH yield of 0.08 [Rebbert & Ausloos 1972]. *Note*: the measurements were at 123.6 nm (yield = 0.059) and 104.8–106.7 nm (yield = 0.23); the estimate at Lyman α is from simple linear interpolation.

These results, along with the requirement that the branching ratios for channels a–e sum to 1.0, are summarized by the following linear equation:

$$\begin{array}{ccccc} 1 & 1 & 1 & 1 & 1 \\ 0 & 0 & 0 & 1 & 0 \\ 0 & 1 & 1 & 0 & 0 \\ 2 & 0 & 1 & 1 & 2 \\ 0 & 0 & 1 & 0 & 0 \end{array} \times \begin{array}{c} q_a \\ q_b \\ q_c \\ q_d \\ q_e \end{array} = \begin{array}{ll} 1.00 & \\ 0.50 & CH_3 \text{ yield} \\ 0.50 & H_2 \text{ yield} \\ 1.00 & H \text{ yield} \\ 0.08 & CH \text{ yield} \end{array}$$

This matrix is singular, owing to the lack of constraints on ${}^1CH_2$ or ${}^3CH_2$ yields, with channels a and e each yielding two hydrogen atoms. We choose to neglect channel e, which results in the overdetermined system

$$\begin{array}{cccc} 1 & 1 & 1 & 1 \\ 0 & 0 & 0 & 1 \\ 0 & 1 & 1 & 0 \\ 2 & 0 & 1 & 1 \\ 0 & 0 & 1 & 0 \end{array} \times \begin{array}{c} q_a \\ q_b \\ q_c \\ q_d \end{array} = \begin{array}{ll} CH_3 \text{ yield} & (0.45 - 0.55) \\ H_2 \text{ yield} & (0.45 - 0.55) \\ H \text{ yield} & (\geq 1.0) \\ CH \text{ yield} & (0.06 - 0.23) \end{array}$$

We solved this system by a least squares method, allowing for the variations in quantum yields given above, and searched for the "best" solution such that $|1 - \sum_i q_i|$ was minimized. It was necessary to renormalize the branching ratios to a sum of 1.0 once the "best" solution had been found; the loss of initial normalization stems from the dropping of one channel and from the "scatter" associated with the least squares solution technique. The result is

$$\begin{array}{lcl} q_a = 0.212 & & CH_3 \text{ yield} = 0.406 \\ q_b = 0.282 & \Longrightarrow & H_2 \text{ yield} = 0.382 \\ q_c = 0.100 & & H \text{ yield} = 0.930 \\ q_d = 0.406 & & CH \text{ yield} = 0.100 \end{array}$$

To extend these results to other wavelengths, we have adopted the following assumptions and constraints:

- for $\lambda \geq 107$ nm, the branching ratios for the various channels are constant with wavelength (the CH yield is 0.23).
- for longer wavelengths, the CH quantum yield varies linearly with wavelength to reproduce the measured variation, while the CH_3, H_2 & H yields remain independent of wavelength (where energetically allowed).
- $q_a(\lambda > 132) = 0$ and $q_c(\lambda > 133) = 0$.
- photolysis branching ratios sum to 1.0.

The laboratory measurements most needed are (1) the yield of ${}^3CH_2$ or ${}^1CH_2$ and (2) the yield of CH, both at Lyman α.

DATA-MODEL COMPARISONS

K profiles of the form

$$K(z) = K_o \cdot \left(\frac{n_o}{n(z)}\right)^{\beta}$$

with $\beta = 0.5$ (the o-subscript refers to a reference level) are used in generating the models shown in the top panels of the two adjacent figures, since this type of profile has been the one most commonly used in photochemical modeling studies of outer planetary atmospheres (typically blamed on Lindzen [1971] and Hunten [1975]). The fits are determined by the $\lambda_c < 140$ nm channels, and it is apparent that the C_2 hydrocarbon abundances in these models are not consistent with the UVS data. In particular, the model lightcurves with λ_c near 152 nm exhibit more acetylene (C_2H_2) opacity than is consistent with the data (these channels encompass the strong first vibrational member of the 3R–X Rydberg transition). At longer wavelengths, particularly in the egress case, the excess opacity in the models is from ethylene (C_2H_4). At shorter wavelengths, where ethane (C_2H_6) is expected to contribute, the model lightcurves are in fairly good accord with the data (except for the egress case at $\lambda_c = 148.2$ nm, where the second member of the acetylene 3R–X system makes its appearance). Near the 0.5 mbar level, there is a large discrepancy with the IRIS-retrieved mixing ratios; this is attributed to K values in this vicinity too large to maintain the observed abundances.

We subsequently defined K-profiles characterized by a small number of layers over which K is held constant, and explored model fits by varying the width and placement of the constant-K layers. The upper troposphere, lower stratosphere dynamics modeling of Conrath *et al.* [1991] suggests a sluggish overturning timescale on the order of 10^9 s, corresponding to an eddy mixing coefficient value of $\sim 2 \times 10^3$ cm^2 s^{-1}. Photochemical modeling of IRIS measurements of stratospheric acetylene and ethane emissions [Bézard *et al.* 1991; Romani *et al.* 1993] also strongly indicates a requirement for a sluggish lower stratosphere if the observed abundances are to be maintained. In view of this, the lowermost constant-K layer has been constrained to values on the order of 2×10^3 cm^2 s^{-1}, although the extent of this layer has been varied.

We found that a minimum of three constant-K layers are required to give a good fit to the UVS data, with the maximum K values belonging to the middle layer centered near 10^{-2} mbar beneath the primary photochemical zone (where unit optical depth in methane at Lyman α occurs):

$$\begin{aligned} K &= K_1\,, && p \geq p_1 \\ &= K_1 \times \left(\tfrac{p}{p_1}\right)^{\gamma_1}\,, && p_1 > p \geq p_2 \\ &= K_2\,, && p_2 > p \geq p_3 \\ &= K_2 \times \left(\tfrac{p}{p_3}\right)^{\gamma_2}\,, && p_3 > p \geq p_4 \\ &= K_3\,, && p \leq p_4 \end{aligned}$$

where $\gamma_1 = \ln(K_2/K_1)/\ln(p_2/p_1)$ and $\gamma_2 = \ln(K_3/K_2)/\ln(p_4/p_3)$. The placement of the rapid rise in K ($p_1 > p \geq p_2$) is chosen in part to reproduce a ratio of ethane-to-acetylene mixing ratios consistent with the Bézard *et al.* [1991] IRIS analysis and in part to avoid stifling the upward flow of CH_4. Other types of profiles were explored (*e.g.*, the profile form adopted by Yung *et al.* [1984] in their extensive Titan photochemical modeling study), but none were found to lead to fits as successful as models with K profiles defined by the above expression.

The models shown in the lower panels of the adjacent figures illustrate the success (and model limitations) obtained with the latter form for K; constituent opacities for these models are also shown. In the ingress case, models giving good fits for the $\lambda_c < 140$ nm and $\lambda_c > 151$ nm channels consistently failed to provide sufficient opacity at intermediate wavelengths, pointing to either an under-abundance of ethane or the presence of an unmodeled constituent. To gain an idea of the amount of C_2H_6 required to bring about agreement, the ethane mixing ratio profile was scaled by a constant factor; an increase in C_2H_6 abundances by a factor of 4.0 in the model brings the model lightcurves into marginal alignment with the UVS data at $\lambda_c = 144.7$ nm and $\lambda_c = 148.4$ nm, but the agreement at $\lambda_c = 152.1$ nm is now worsened. It is noteworthy, however, that the fit at shorter wavelengths is *not* compromised. It may be that our adoption of "local" conditions is inappropriate for the ingress data. If the rapid mixing in the middle stratosphere indicated by our models is a manifestation of advection in a meridional circulation system, then the photochemical stability of ethane would suggest that its abundance should be more reflective of global solar illumination conditions.

The egress models are inherently close to such illumination conditions, and generating ethane abundances within the models sufficient to account for the opacities measured by the UVS is not difficult, using the K-profile form with 3 constant layers. In the egress case, however, as in the ingress case, it is difficult to obtain consistent fits across the 140–153 nm interval, since ethane abundances yielding good fits at 140–148 nm result in too much total opacity at 152 nm where the acetylene spectral signature lies. In the adjacent figure we show a compromise fit geared toward giving agreement with the IRIS-retrieved C_2H_6 mixing ratio at 0.7 mbar while maintaining a marginally acceptable fit to the UVS 152 nm lightcurve. A factor of $\sim$3 discrepancy with the IRIS acetylene results is noted.

The K value in the middle layer is the minimum value needed in the models to prevent excessive C_2H_4 abundances *vis-a-vis* the data at wavelengths $\lambda_c > 153$ nm. Why is an enhanced K necessary? – briefly, to transport C_2H_4 out of the primary photochemical zone where it is produced mainly by R3 ($CH + CH_4 \rightarrow C_2H_4 + H$) to deeper levels where it is consumed in the three body reaction R11 ($C_2H_4 + H + M \rightarrow C_2H_5 + M$). The subsequent fate of C_2H_5 is R12 ($C_2H_5 + H \rightarrow CH_3 + CH_3$), after which the methyl radical can combine with itself to form ethane (R6). Thus, enhanced K values in the vicinity of the primary photochemical zone (and beneath the nominal homopause) also contribute to ethane production. Even with $K \gtrsim 10^8$ cm^2 s^{-1} in the middle layer, we have found it necessary to adopt a fast rate for R11. Nevertheless, the inference of the existence of a region of enhanced eddy mixing at pressures beneath the nominal homopause is not critically dependent on the particular reaction rates we have adopted; it is based directly on the strong limits placed on ethylene abundances by the UVS data and on the displacement between C_2H_4 production and loss zones.

At both ingress and egress, the placement of the "rapid-rise" in K is roughly consistent with the analysis of probable wave signatures in the RSS occultation data by Hinson and Magalhães [1993]. However, we are not in a position to explain the large values of K in the middle layer of our models in terms of a particular mixing mechanism; in this work, K is simply a fitting parameter. However, it is our belief that, by and large, the chemistry is well accounted for, at least to the extent that our ignorance of dynamical conditions in Neptune's stratosphere introduces greater uncertainties in modeling than remaining uncertainties in key reaction rates. If so, then our K-profiles yielding good agreement between models and data should provide useful constraints in dynamical modeling studies.

To see if we could improve upon the model fits shown above, we have constructed models using piecewise constant K profiles partitioned by scale height above the tropopause. Given the rather large number of free parameters (more than can be uniquely specified by the data), we have simply patterned these K-profiles on our previous results and attempted to refine the fits with the data. Typical results are shown in the adjacent figure. It has not been possible (as yet) to improve upon the models based on K profiles of the 3-constant-layers variety, suggesting that more sophisticated models are not warranted by the data. The relative under-abundance of ethane is still apparent in the ingress model. The egress model was geared toward agreeing with both the IRIS C_2H_6 and C_2H_2 data points while remaining marginally consistent with the UVS data over the 140–153 nm range; the most obvious difficulty is with the UVS 151.9 nm channel, owing to the abundance of acetylene required by the IRIS data.

This analysis is continuing.

Left Panels: thick solid curve, eddy mixing coefficient; solid curve, CH_4 mixing ratios; long-dash curve, C_2H_6 mixing ratios; short-dash curve, C_2H_2 mixing ratios; dotted curve, C_2H_4 mixing ratios. Scaled ethane mixing ratio profiles are shown in red. Altitudes referenced to 1 bar radius of 24445 km (nominal atmosphere).
Right Panels: solid curves, model I/I_o lightcurves; blue histograms, UVS data $I/I_o \pm \sigma$. Lightcurves generated using scaled ethane mixing ratios are shown in red. Channel center wavelengths at 500 km minimum tangent ray height (MTRH) are indicated.

Ingress: Conventional K-Profile

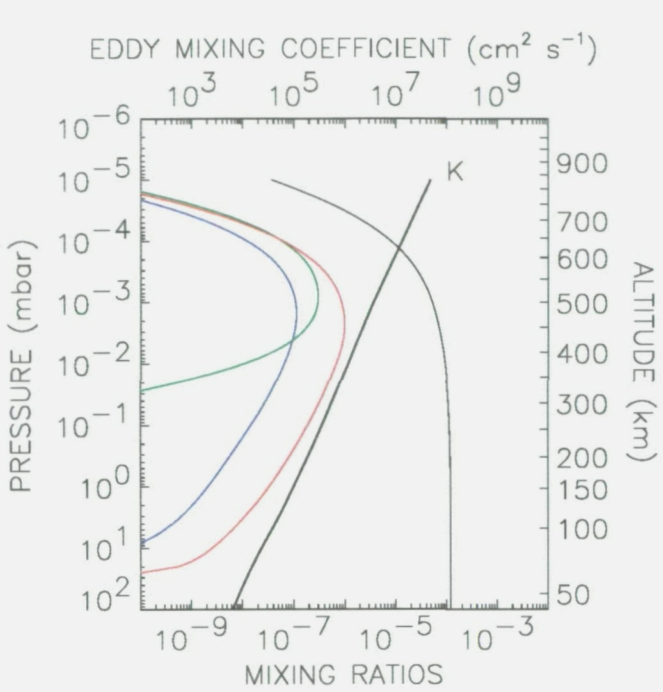

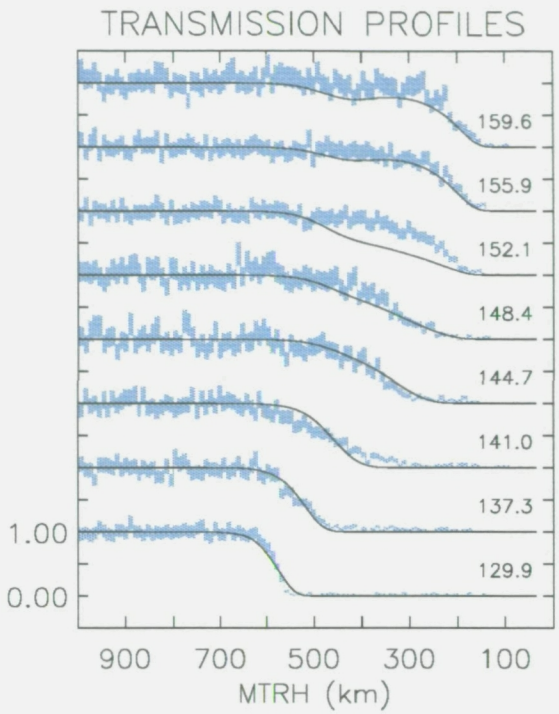

Ingress: K-Profile with 3 Constant Layers

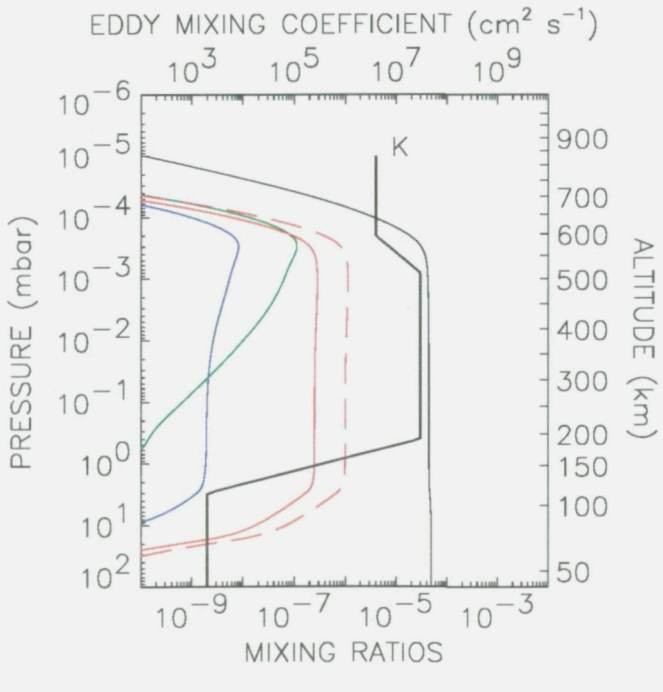

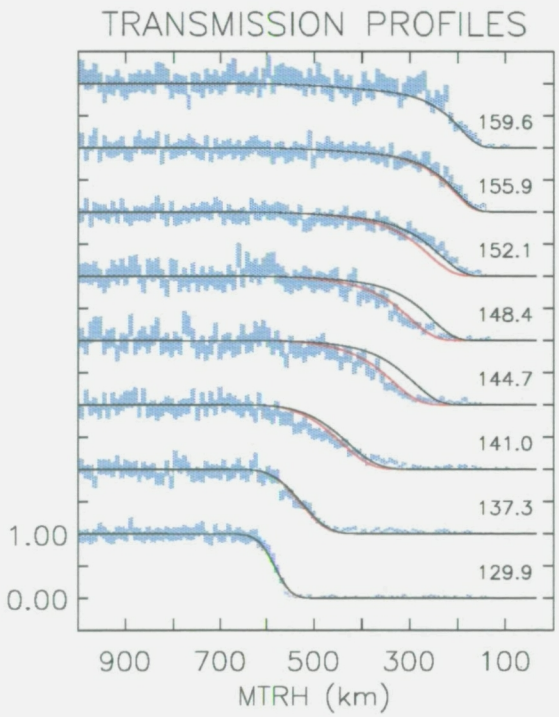

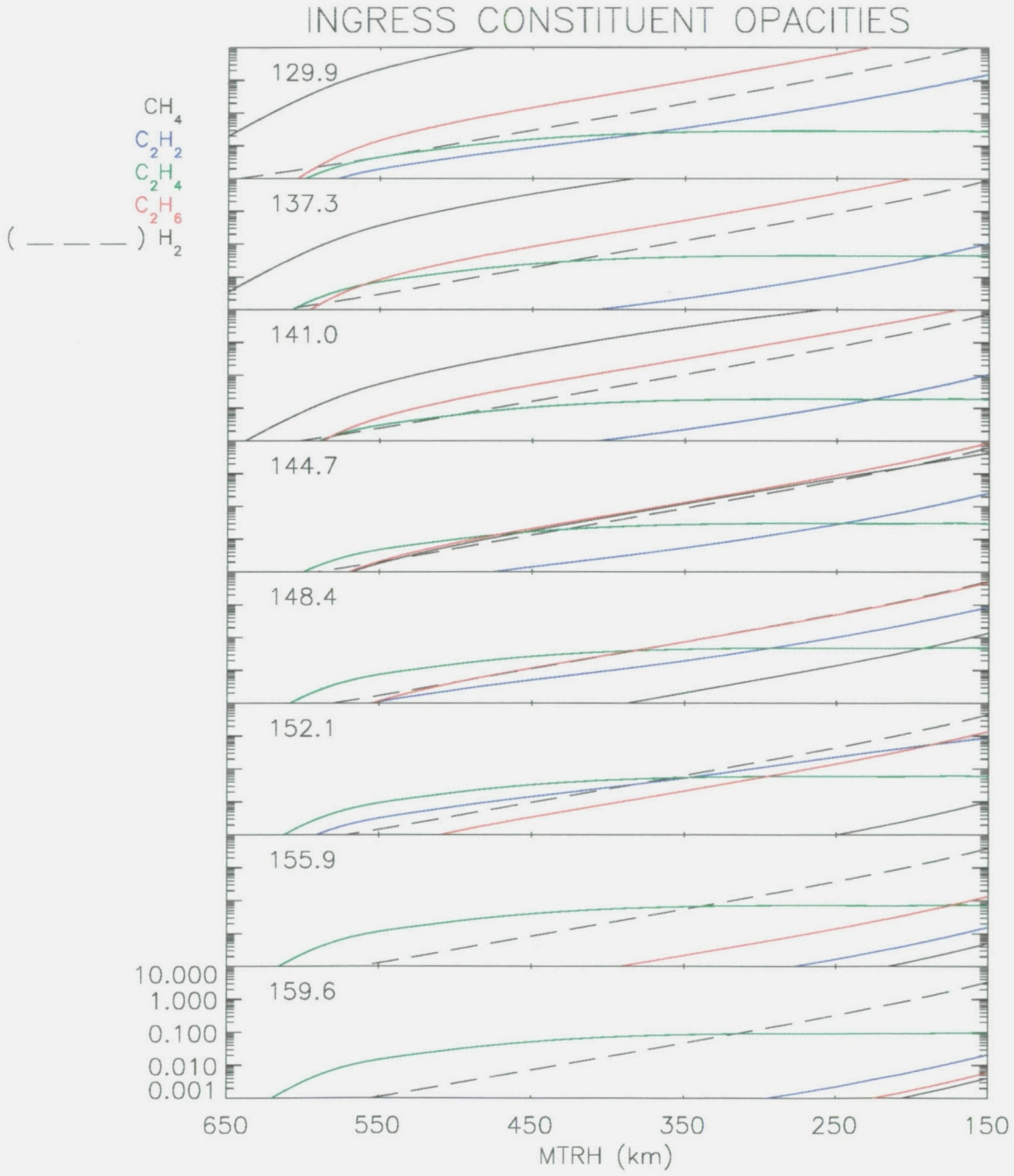
INGRESS CONSTITUENT OPACITIES
CH4
C2H2
C2H4
C2H6
(— — —) H2
129.9
137.3
141.0
144.7
148.4
152.1
155.9
159.6
10.000
1.000
0.100
0.010
0.001
650
550
450
350
250
150
MTRH (km)

Egress: Conventional K-Profile

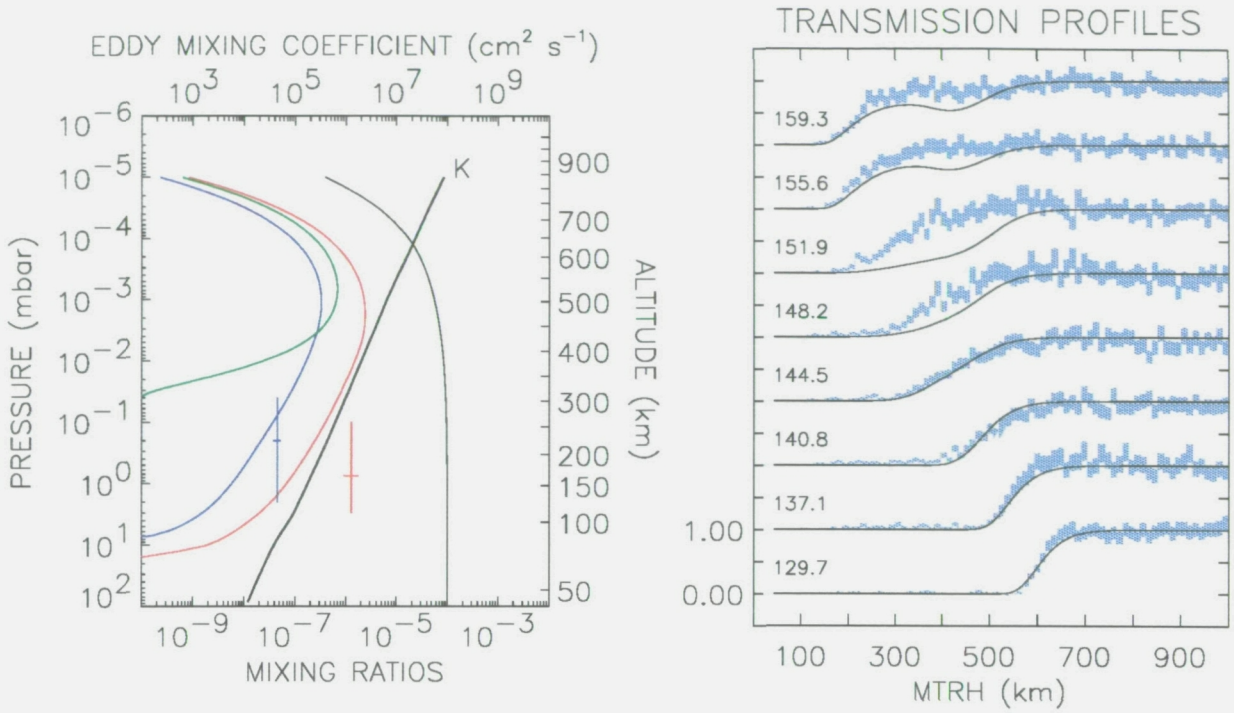

Egress: K-Profile with 3 Constant Layers

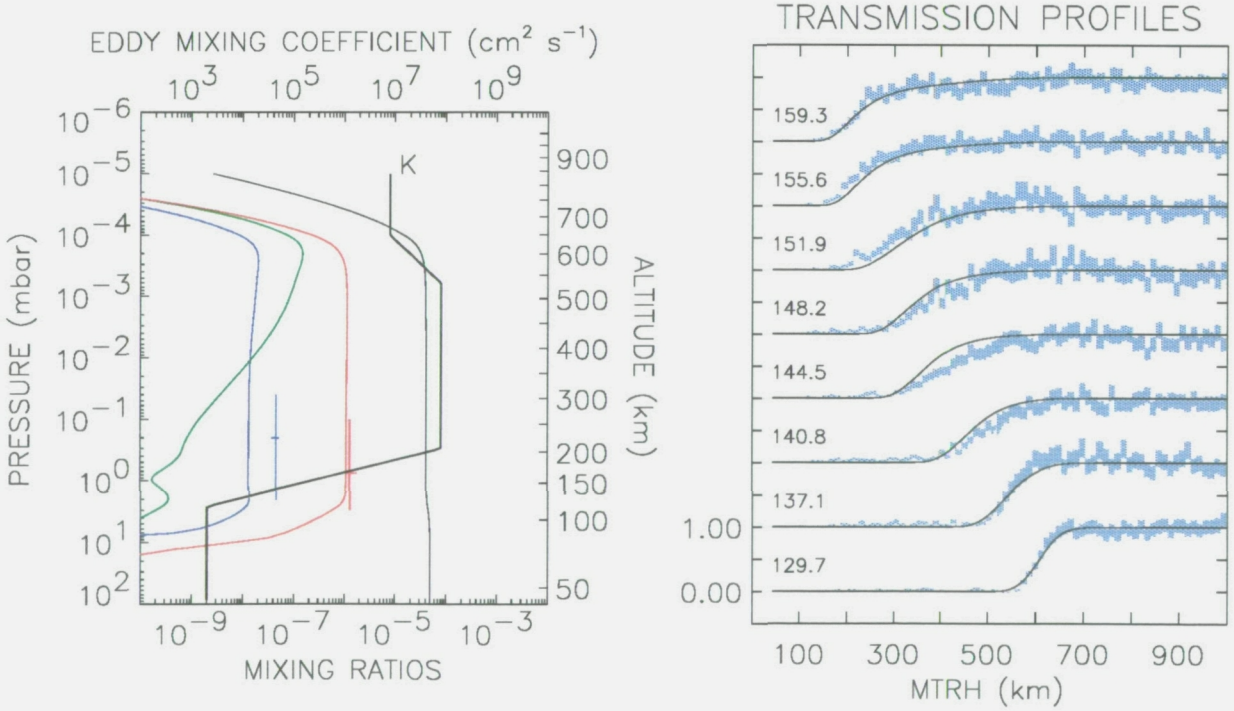

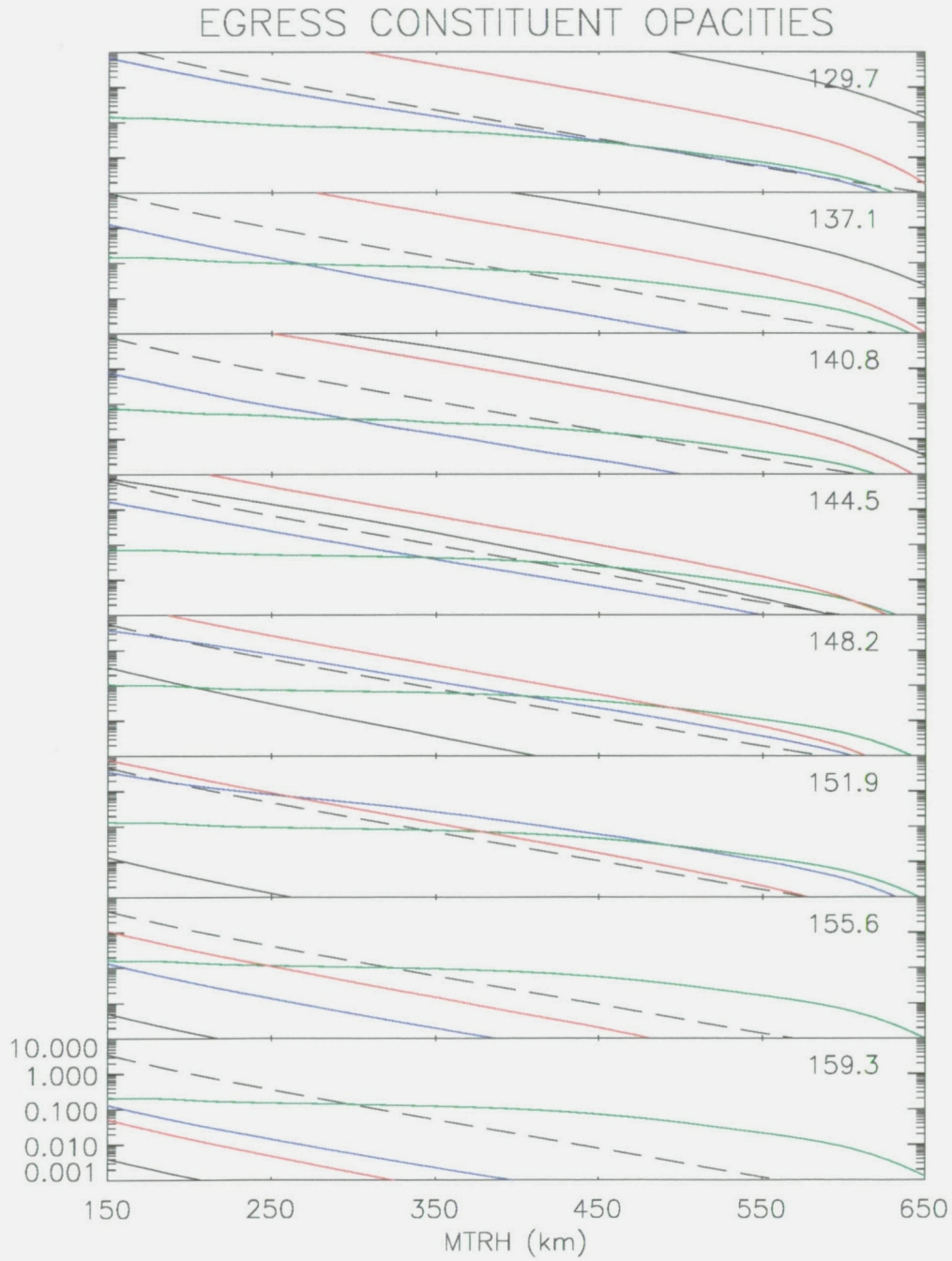
EGRESS CONSTITUENT OPACITIES
129.7
137.1
140.8
144.5
148.2
151.9
155.6
159.3
10.000
1.000
0.100
0.010
0.001
150
250
350
450
550
650
MTRH (km)

Ingress: Example with constant K per scale height

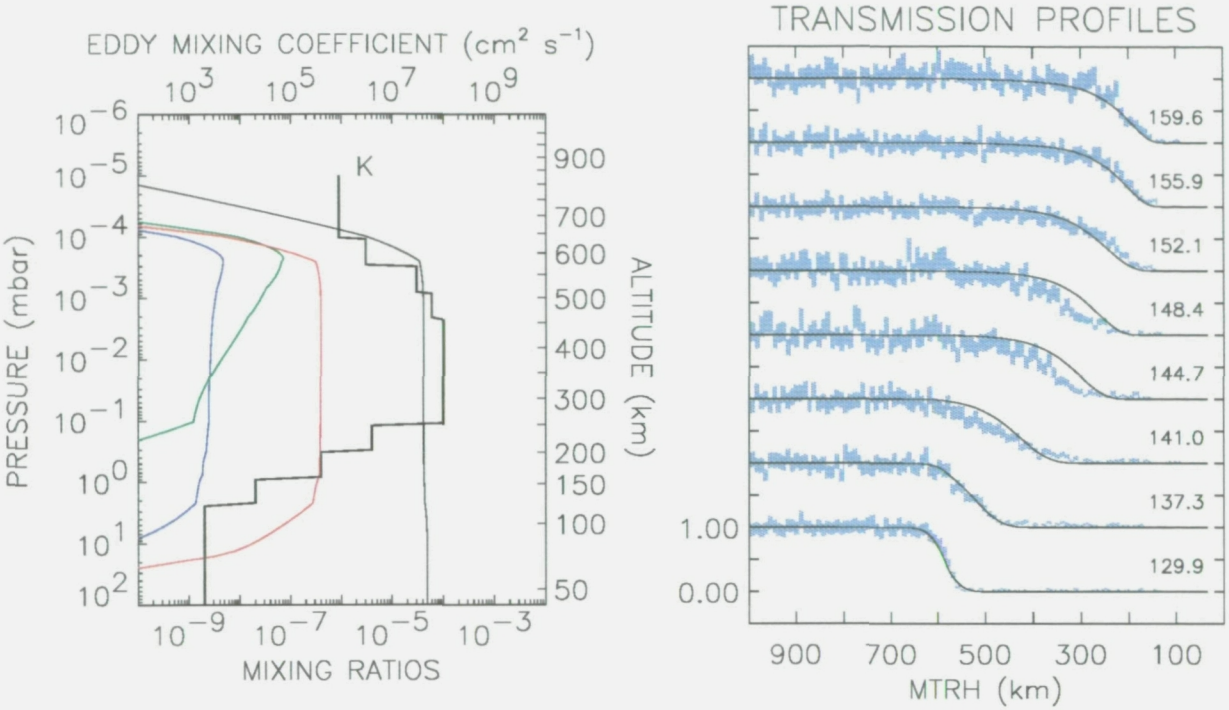

Egress: Example with constant K per scale height

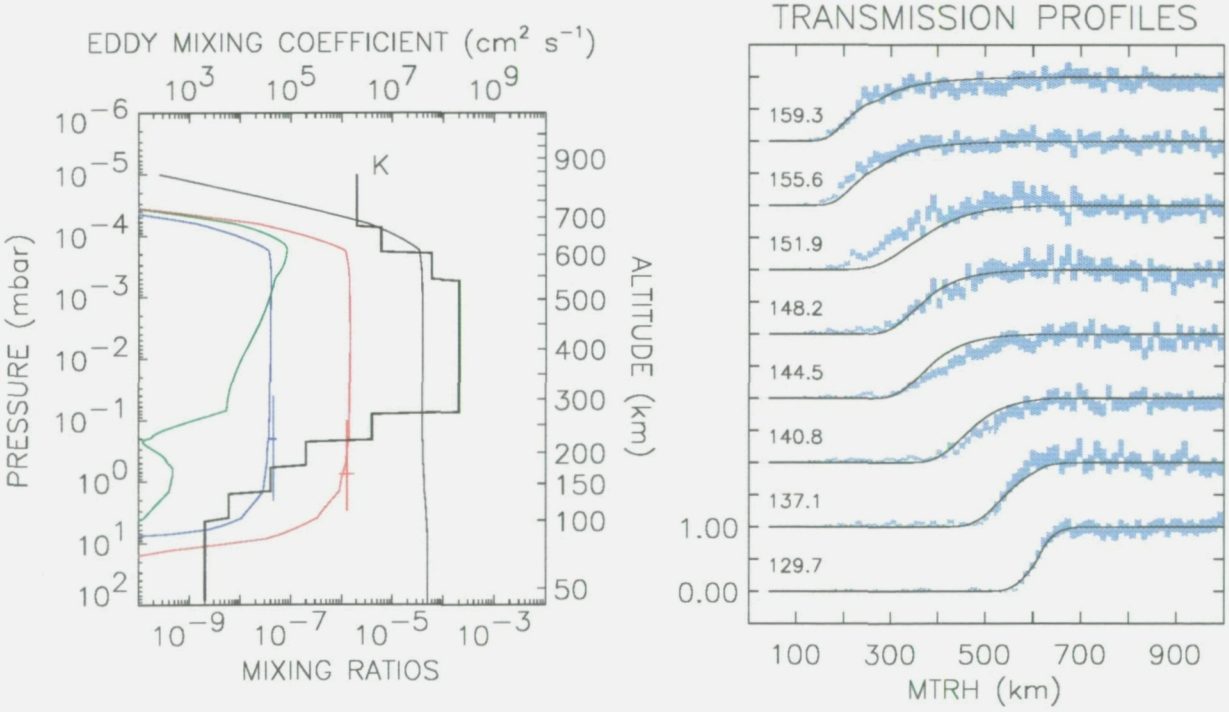

ICARUS 106, 442–463 (1993)

ATTACHMENT 3

Methane Photochemistry on Neptune: Ethane and Acetylene Mixing Ratios and Haze Production

PAUL N. ROMANI

Mail Code 693, NASA–Goddard Space Flight Center, Greenbelt, Maryland 20771
E-mail: ys2pr@viris.dnet.nasa.gov

JAMES BISHOP

Computational Physics Inc., 2750 Prosperity Avenue, Suite 600, Fairfax, Virginia 22031

BRUNO BÉZARD

Observatoire de Paris, Section de Meudon, Département de Recherche Spatiale, 92195 Meudon, France

AND

SUSHIL ATREYA

Department of Atmospheric, Oceanic and Space Sciences, University of Michigan, Space Research Building, Ann Arbor, Michigan 48109-2143

Received October 1, 1992; revised September 16, 1993

We have used a one-dimensional methane photochemical model to analyze Voyager observations of hydrocarbons and hazes in the stratosphere of Neptune. Voyager IRIS spectra provide information about the global average C_2H_2 and C_2H_6 mixing ratios for $p > 0.1$ mbar. The UVS lightcurves provide constraints on CH_4 and C_2H_4 in addition to C_2H_2 and C_2H_6 but only at the solar occultation latitudes and for lower pressures. The model-predicted hydrocarbons are very sensitive to the height profile of the eddy diffusion coefficient (K). For both data sets K varying inversely with the atmospheric number density to some power produced poor results. Good agreement with the data requires that K be weak in the lower stratosphere ($K \approx 2 \times 10^3$ cm^2 sec^{-1} for $p \gtrapprox 2$ mbar) but fairly vigorous in the upper stratosphere ($K \geq 5 \times 10^7$ cm^2 sec^{-1} for $p \lessapprox 0.5$ mbar), i.e., a rapidly mixed upper stratosphere overlying a stagnant lower stratosphere with a rapid transition in between. The model C_2H_6 and C_2H_2 mixing ratios are also sensitive to the reaction rate constants of $C_2H_4 + H$ and $CH_3 + C_2H_3$. Notably, we must use the present upper limit for the $C_2H_4 + H$ rate to best fit the model results to the observations. We are able to reproduce the IRIS C_2H_2 and C_2H_6 emission features well, less so the UVS occultation lightcurves. Since the transport of C_2H_2, C_2H_6, and other hydrocarbons produced from methane photolysis out of the stratosphere is by ice haze formation and sedimentation, we compared model haze predictions to PPS and IRIS observations. For solar maximum fluxes (Voyager encounter conditions) the model mass production rate is 1×10^{-14} g cm^2 sec^{-1}. C_2H_6 is the dominant haze component (75%), with the remainder coming from C_2H_2 and C_3 and C_4 compounds. Balancing the above haze production rate by the sedimentation rate for 0.25-μm radius particles (upper limit to particle radius from PPS observations) yields a total haze column burden slightly above the PPS upper limit. However, lifetime analysis indicates that the model haze production rate should be averaged over solar minimum and maximum conditions. Under these conditions the model haze density is consistent with the PPS data. The predicted C_4H_2 and C_2H_6 haze column densities are consistent with the lack of ice signatures in the IRIS spectra.

I. INTRODUCTION

Methane (CH_4) and its photochemical products acetylene (C_2H_2) and ethane (C_2H_6) have been observed in emission in the infrared from Neptune's stratosphere for over 10 years (see references in Orton and Appleby 1984, and Kostiuk *et al.* 1992). The retrieved mole fractions of these species are much greater than their respective saturation mixing ratios at the tropopause. This, coupled with observational evidence of a lower stratospheric haze ($p > 5$ mbar) on Neptune (see, e.g., Baines and Smith 1990, Hammel *et al.* 1989), naturally led to the speculation that these and potentially more complex hydrocarbons were the source for the haze.

An understanding of these hydrocarbons and hazes is important to an understanding of the carbon cycle in the stratosphere of Neptune. Carbon, in the form of methane,

0019-1035/93 $5.00

REFERENCES

Bézard *et al.* [1991] *J. Geophys. Res.* **96**:18961.
Bishop *et al.* [1992] *J. Geophys. Res. Planets* **97**:11681.
Broadfoot *et al.* [1989] *Science* **246**:1459.
Bruckner *et al.* [1993] *J. Geophys. Res.* **98**:10695.
Conrath *et al.* [1991] *J. Geophys. Res.* **96**:18907.
Conrath *et al.* [1991] *J. Geophys. Res.* **96**:18931.
Glicker and Okabe [1987] *J. Phys. Chem.* **91**:437.
Hinson and Magalhães [1993] *Icarus* **105**:142.
Hinteregger *et al.* [1981] *Geophys. Res. Lett.* **8**:1147.
Hubbard *et al.* [1987] *Icarus* **72**:635.
Hunten [1975] in *Atmospheres of the Earth and Planets*, B. M. McCormac, ed., 59 (Reidel).
Laufer and McNesby [1968] *J. Chem. Phys.* **49**:2272.
Lee and Chiang [1983] *J. Chem. Phys.* **78**:688.
Lindal [1992] *Astron. J.* **103**:967.
Lindzen [1971] in *Mesospheric Models and Related Experiments*, G. Fiocco, ed., 122 (Reidel).
Mordaunt *et al.* [1993] *J. Chem. Phys.* **98**:2054.
Moses *et al.* [1992] *Icarus* **99**:318.
Mount and Moos [1978] *Astrophys. J.* **224**:L35.
Mount *et al.* [1977] *Astrophys. J.* **214**:L47.
Orton *et al.* [1992] *Icarus* **100**:541.
Rebbert and Ausloos [1972] *J. Photochem.* **1**:171.
Romani *et al.* [1993] *Icarus* **106**:442.
Roques *et al.* [1994] *Astron. Astrophys.* **288**:985.
Slanger and Black [1982] *J. Chem. Phys.* **77**:2432.
Suto and Lee [1984] *J. Chem. Phys.* **80**:4824.
Wu *et al.* [1989] *J. Chem. Phys.* **91**:272.
Yelle *et al.* [1993] *Icarus* **104**:38.
Yung *et al.* [1984] *Astrophys. J. Supp.* **55**:465.